Peripheral spatial vision: limits imposed by optics, photoreceptors, and receptor pooling

Martin S. Banks, Allison B. Sekuler,* and Stephen J. Anderson†

School of Optometry and Department of Psychology, University of California, Berkeley, Berkeley, California 94720

Received June 14, 1990; revised manuscript received June 17, 1991; accepted June 17, 1991

We examined the contribution of optical and photoreceptor properties as well as receptor pooling to eccentricity-dependent variations in spatial vision by comparing the performance of ideal observers with that of human observers. We measured contrast sensitivity functions in human observers and calculated such functions in ideal observers for retinal eccentricities of 0–40 deg. Comparisons of human and ideal performance in a variety of tasks reveal that many aspects of the variation in spatial vision with eccentricity can be understood from an analysis of the discrimination information available at the retinal ganglion cells.

INTRODUCTION

Optical, photoreceptor, retinal, and higher-order neural factors combine to determine visual performance, but it is frequently difficult to determine the relative contributions of these factors because they cannot be independently manipulated. These factors vary with retinal eccentricity, however, so the study of variations in spatial vision across the visual field might provide key insights into how optical, receptoral, and neural properties limit performance.

Several features of the visual system, including optical quality,[1] the size and the shape of individual cones,[2] cone packing density,[2,3] the convergence of cones onto retinal neurons,[4] and the magnification of retinal-to-cortical connections,[5] vary with eccentricity. Visual performance also varies dramatically with eccentricity, and there are two views of the variations. One holds that the degradation of spatial vision with eccentric viewing is quantitative: A single spatial scaling factor is sufficient to equate performance across eccentricities.[6,7] According to this view, the accuracy and the character of visual performance are the same at all eccentricities, except for differences in the size of underlying mechanisms. The other view holds that the degradation of vision with eccentricity is qualitative: No single scaling factor can equate performance across eccentricities. The fact that vernier acuity falls two or three times more rapidly with eccentricity than does grating acuity[8,9] is one piece of evidence for the latter view. Indeed, Levi *et al.*[9] have argued from such observations that different structures limit grating and vernier acuity. They claim that the variation in grating acuity is due mostly to optical and retinal factors and that the variation in the hyperacuities is due mostly to cortical factors.

We examined the contribution of optical and photoreceptor properties to eccentricity-dependent variations in spatial vision by relating the performance of ideal observers to that of human observers. The performance of an ideal observer is the best possible in the presence of photon noise, so such performance is a measure of the discrimination information available at a chosen processing site.[10] By calculating the performance of an ideal observer placed at the receptors, we can estimate how variations in optical quality and in receptor density, optics, and efficiency affect the discrimination information available to the rest of the visual system. By comparing ideal and human performance, we can estimate how much of the variation in human performance can be explained by information losses at the outputs of the receptors themselves.

Banks *et al.*[11] used this approach to examine the physical limits of contrast sensitivity in the fovea. They found that the high-frequency slope of the foveal contrast sensitivity function (CSF) can be explained by the operation of preneural factors (optics and photoreceptor properties) plus variations in grating summation area. In the present study we measured CSF's in human observers and calculated such functions in ideal observers for eccentricities of 0–40 deg. We also examined grating and vernier acuity and spatial summation. We found that many, but by no means all, aspects of the variation in spatial vision with eccentricity can be understood from an analysis of the discrimination information available at the receptors. We then pushed the analysis further along the visual pathway by including receptor pooling (the convergence of cones onto higher-order retinal neurons) and showed that a great deal of the eccentricity dependence of spatial vision can be understood from the information at that stage.

GENERAL METHODS

Stimuli and Procedure

The stimuli in all but Experiment 3 and parts of Experiment 4 below were horizontal Gabor patches presented either foveally or in the nasal visual field along the horizontal meridian. The display was a Joyce Electronics cathode-ray tube with a P4 phosphor, and the space-average luminance was 762 cd/m^2. We used a range of viewing distances to ensure that the spatial transfer function of the CRT did not affect the contrasts of targets at different spatial frequencies. Either a small black spot on the cathode-ray tube or a LED served as a fixation target. We varied retinal eccentricity by changing the position of the spot or the LED.

0740-3232/91/111775-13$05.00

Two well-practiced observers—an emmetrope and a 0.75-D myope—viewed the stimuli monocularly through a 1.5-mm artificial pupil. Retinal illuminance was 1348 Td. Head position was stabilized with a bite bar, and accommodation was paralyzed with 1% cyclopentolate. Alignment of the artificial pupil and optical correction were accomplished in the following way. For each eccentricity and viewing distance, the observers adjusted the position of the pupil vertically and horizontally (using a two-dimensional microscope stage) and inserted ophthalmic lenses of different powers (in 0.12-D steps) placed close to the cornea. The observers identified the combination of pupil position and lens power that maximized the perceived contrast of a horizontal grating patch with spatial frequency near the acuity cutoff. Any residual errors in optical correction are unlikely to have affected our findings because the depth of focus is large with 1.5-mm pupils.[12]

Each trial was initiated by the observer and consisted of two 100-ms intervals of abrupt onset and offset. The two intervals were marked by tones and were separated by 250 ms. The observer identified the interval that contained the grating patch. He or she could also discard a trial if Troxler's fading or some other difficulty was experienced. Auditory feedback indicating the accuracy of the observer's response was given after each trial.

Contrast was varied according to the method of constant stimuli. Threshold was defined as the contrast associated with the 75% correct point on each psychometric function and was estimated by probit analysis. Grating acuity thresholds were estimated by varying the spatial frequency of a grating patch of 50% contrast according to a two-down/one-up staircase.

Construction of Ideal Observers

Following Geisler,[13] we built ideal observers with the optics and photoreceptor properties of the human eye at 0, 2, 5, 10, 20, and 40 deg along the horizontal meridian in the nasal visual field.

In regard to optics, three properties were considered: effective pupil size, ocular media transmittance, and the optical transfer function (OTF). The effective pupil size for each eccentricity was calculated and built into the appropriate ideal observer. Although OTF measurements as a function of eccentricity have been published,[1] we found in preliminary studies that these measurements probably underestimated the quality of peripheral optics in our two observers. Thus we used a 1.5-mm artificial pupil in order to render the optics diffraction limited. We then calculated the OTF from equations for perfect, diffraction-limited lenses and white light.[14] The OTF's were, therefore, identical at all eccentricities.

In regard to photoreceptor properties, we used anatomical data from Curcio *et al.*[2] to estimate intercone spacing and the diameter of cone inner segments as a function of eccentricity. In addition, we used data from Polyak[15] and from Cheng-Yu and Van Sluyters[16] for cone outer-segment lengths and diameters. These dimensions are summarized in Fig. 1. With increasing eccentricity, intercone spacing and inner-segment diameter increase, outer-segment length decreases, and outer-segment diameter varies little. The size of the effective aperture in peripheral cones has not been established, but MacLeod and colleagues[17] argue from psychophysical observations that it is correlated with, though noticeably smaller than, the diameter of the inner segment at the external limiting membrane. Because of the lack of resolution on this point, we will provide two calculations, one assuming that inner segments at the external limiting membrane are the effective aperture and one assuming that outer segments are. The true state of affairs probably lies between these two extremes.

Several cone lattice properties vary with retinal eccentricity: In addition to intercone spacing, these include retinal coverage and optical density. Some consequences of these eccentricity-dependent variations are depicted in Fig. 2. The left-hand panel plots retinal coverage, which is the percentage of retinal area covered by cone apertures. Clearly, retinal coverage declines significantly with eccentricity whether one assumes that the inner or the outer segment is the effective cone aperture in the periphery. The change in optical density with eccentricity is a consequence of the shorter outer segments of peripheral cones. We used standard equations[18] to calculate the isomerization rate of cone outer segments in different retinal regions. We assumed that cone outer segments at

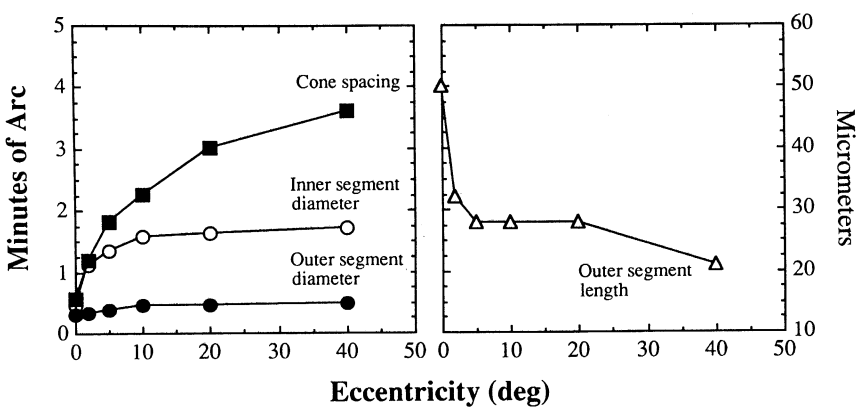

Fig. 1. Cone lattice properties at different retinal eccentricities. Left: Intercone spacing and inner- and outer-segment diameters in minutes of arc. The intercone spacing estimates are from Curcio *et al.*[2]; a regular triangular arrangement of cones was assumed in calculating the values shown. Inner-segment diameters were measured at the external limiting membrane by Curcio *et al.*[2] Outer-segment diameters are from some recent measurements by Cheng-Yu and Van Sluyters[16]; they are consistent with values reported by Polyak.[15] Right: Outer-segment lengths in micrometers. These data are from recent measurements by Cheng-Yu and Van Sluyters[16] and are consistent with those of Polyak.[15]

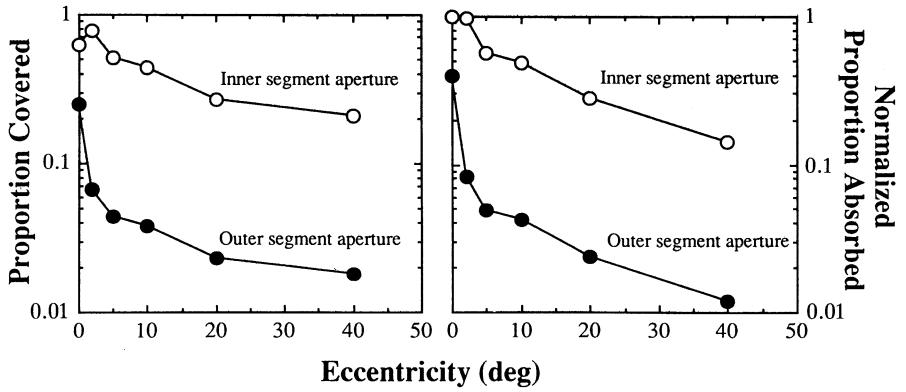

Fig. 2. Cone lattice coverage and efficiency at different eccentricities. Left: Retinal coverage, the percentage of retinal area covered by cone inner or outer segments, is plotted as a function of eccentricity. A regular triangular arrangement of cones was assumed in calculating these values. Two curves are shown, one drawn assuming that inner segments are the effective apertures and one assuming that outer segments are. Right: Proportion of quanta incident upon the cone lattice that is effectively absorbed at different eccentricities. The ordinate has been normalized so the foveal absorption rate (assuming inner-segment apertures) is 1.0. These curves take into account the variation in retinal coverage shown in the left-hand panel. We used Beer's law equations[18] to calculate the isomerization rate in different retinal regions. We assumed that outer segments at different eccentricities differ only in their lengths (that is, that the concentrations and extinction coefficients of photopigment are the same).

different eccentricities differ only in their lengths (that is, that the concentrations and extinction coefficients of photopigment are the same). By our calculations, the isomerization rate of cone outer segments at 40-deg eccentric is 0.25 log unit lower than that of foveal outer segments.

The right-hand panel of Fig. 2 plots the relative quantum catch of cone lattices at different eccentricities. The reduced retinal coverage and isomerization rate of peripheral cone lattices reduces efficiency in converting photons into isomerizations relative to the foveal cone lattice. If one assumes that inner segments are the effective cone aperture throughout the retina, peripheral lattices are roughly 1 log unit less efficient than the foveal lattice in converting incident light into isomerizations. If one assumes that outer segments are the effective apertures, the periphery is approximately 1.6 log units less efficient.

The photoreceptor properties illustrated in Figs. 1 and 2 were built into the ideal observers. Because the effective cone aperture appears to be smaller than the inner segment but larger than the outer segment,[17] we built two ideal observers at each eccentricity: one assuming that inner segments at the external limiting membrane were the effective aperture and one assuming that outer segments were.

Finally, we needed to consider grating summation effects. Ideal observers summate perfectly across space and time, but humans do not. To avoid contamination of comparisons of human and ideal sensitivity, we decided to use target durations within the temporal integration time of the visual system and to use target patch sizes small enough to lie within the spatial integration area for contrast detection. In regard to temporal properties, we found in preliminary experiments that 100-ms rectangular pulses were suitable for all eccentricities and spatial frequencies. It was evident from the literature[19] that we would have to vary the spatial extents of the targets with eccentricity and spatial frequency. For this reason, we conducted an experiment in which we measured the relationship between the spatial extent of the grating patch and the contrast sensitivity for the conditions of the main experiment. The goal was to determine the largest grating patch, for each experimental condition, for which summation was complete.

EXPERIMENT 1

Methods

We measured grating summation functions[20] by presenting Gabor functions of varying spatial extents (but equal height and width). The stimuli were as described in the General Methods section of this paper. Contrast sensitivity was measured as a function of the number of grating cycles in the Gabor patch at the eccentricities of the main experiments. We presented three to six patch sizes at each of two to four spatial frequencies at each eccentricity.

Results

Figure 3 displays the resulting grating summation functions at two spatial frequencies for an eccentricity of 10 deg. The grating summation curves for the ideal observers are lines with a slope of 1. Notice that the slope of the data was ~1 for small numbers of cycles, indicating complete summation. We wished in our main experiment to present the largest grating patch for which summation is complete. To locate this point, we fitted the data with

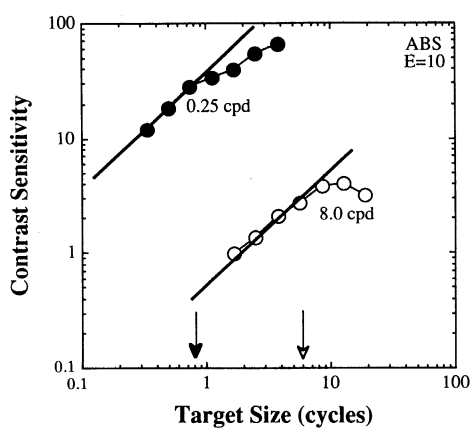

Fig. 3. Grating summation functions at an eccentricity of 10 deg. Contrast sensitivity is plotted as a function of target size in cycles. Target size refers to two standard deviations of the Gaussian envelope. The lines have slopes of 1 and represent the effect of manipulating target size when complete summation holds. We located the point at which the data first deviated from the complete summation lines. The arrows indicate the target sizes at those points.

a line of slope 1, as shown, and defined the critical summation size as the point at which the slope of the data first fell below the line. Those summation sizes, which were used in the main experiment, are given in Table 1 for all the conditions tested.

EXPERIMENT 2

The main experiment reported here involved measurements of contrast sensitivity from 0 to 40 deg. The resulting CSF's were then compared with the CSF's of ideal observers with the optical and photoreceptor properties of different retinal eccentricities.

Methods

We measured CSF's by presenting horizontal Gabor functions along the horizontal meridian. Observer ABS was tested at 0, 5, 10, 20, and 40 deg; observer SJA was tested at 2, 10, and 40 deg. The stimuli were as described in the General Methods section. The standard deviations of the Gabor functions were determined from the results of Experiment 1. Table 1 shows the target sizes expressed as numbers of cycles contained in two standard deviations.

Contrast thresholds were estimated with a two-interval forced-choice procedure in which contrast was varied according to the method of constant stimuli. Percentage correct was determined for four or five contrasts at each spatial frequency with 50–100 observations at each contrast. The highest frequency point on each CSF was obtained by varying the spatial frequency of a grating patch of 50% contrast according to a two-down/one-up staircase with 12 reversals. Four or more such staircases were run to estimate this point.

Results

Figure 4 shows CSF's for both observers at each eccentricity tested. With increasing eccentricity, contrast sensitivity falls off at progressively lower spatial frequencies. The high-frequency cutoffs range from approximately 2.5 cycles per degree (cpd) at 40 deg to 35 cpd in the fovea. Low-frequency sensitivity is similar from one eccentricity to the next, with the exception of the foveal data. Later in this section we hypothesize that the steeper low-frequency falloff of the foveal CSF was caused by an experimental artifact. With the exception of the foveal data, the CSF's of Fig. 4 can be nearly superimposed by shifting them along the log spatial frequency axis (see also Ref. 6).

Figure 5 displays ideal CSF's for the stimulus conditions of the present experiment. Functions in the left-hand panel are based on the assumption that cone inner segments are the effective receptor aperture, and those in the right-hand panel on the assumption that outer segments are. We plot both because, as we mentioned above, the effective cone aperture may be between the inner- and outer-segment diameters.[17,21] In both panels, ideal con-

Table 1. Target Size (number of cycles)

		Eccentricity (deg)				
Spatial Frequency	Fovea	2	5	10	20	40
0.25	–	–	1.00	0.80	1.70	1.70
0.40	0.80	–	1.21	1.00	1.70	1.70
0.65	1.05	1.00	1.51	1.49	1.81	1.70
1.0	1.20	1.30	1.71	2.00	1.90	1.70
1.6	1.35	1.70	2.20	2.39	2.00	1.70
2.6	1.50	2.40	2.50	3.02	2.00	–
4.0	1.75	3.20	3.40	3.99	2.00	–
6.5	1.90	3.21	4.19	4.50	–	–
8.0	–	–	–	4.50	–	–
10.0	2.03	3.79	4.80	–	–	–
16.0	2.05	3.99	–	–	–	–
26.0	2.05	4.22	–	–	–	–

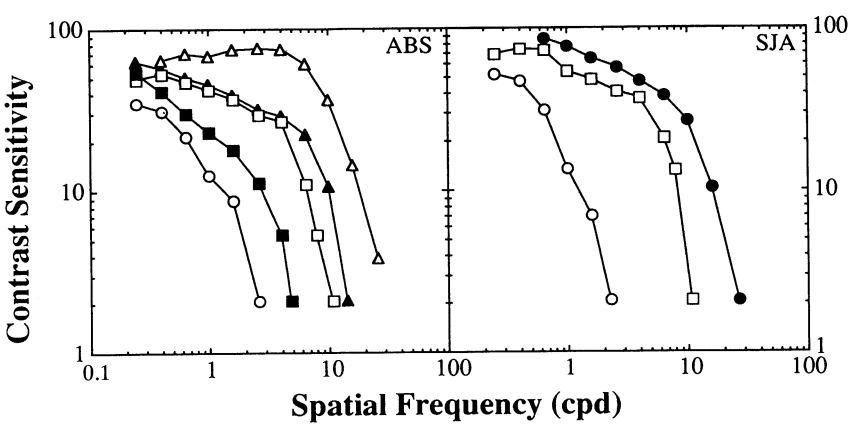

Fig. 4. CSF's at different eccentricities. The left- and right-hand panels display CSF's from observers ABS and SJA, respectively: open triangles, fovea; filled circles, 2 deg eccentric; filled triangles, 5 deg; open squares, 10 deg; filled squares, 20 deg; open circles, 40 deg. Experimental conditions are described in the text and Table 1.

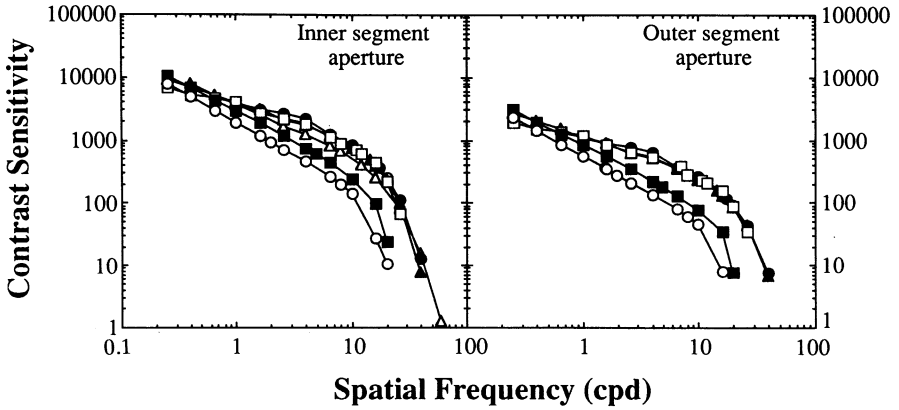

Fig. 5. Ideal CSF's at different eccentricities. The left-hand panel displays ideal CSF's assuming that the inner segment is the effective cone aperture. The right-hand panel shows ideal CSF's assuming outer-segment apertures. The same symbol conventions as in Fig. 4 are used. The properties of the ideal observers at different eccentricities are described in the text and in Table 1.

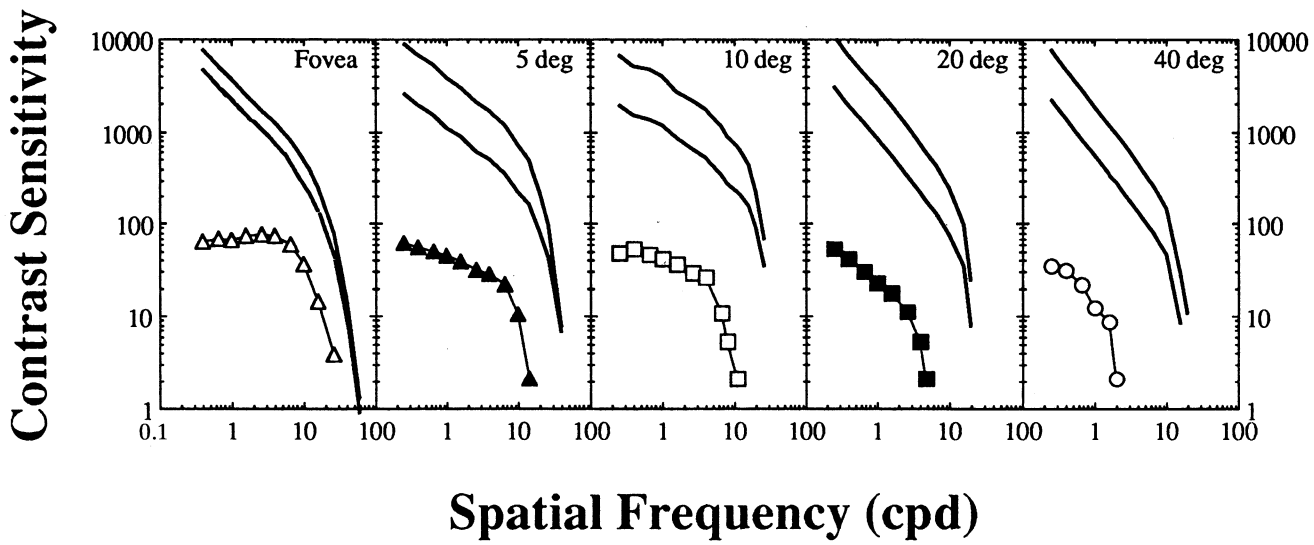

Fig. 6. Human and ideal CSF's at different eccentricities. The panels display functions at 0, 5, 10, 20, and 40 deg eccentric. The symbols represent the data, and the solid curves represent the ideal observer sensitivity functions. Two ideal functions are shown at 5–40 deg; the upper curve represents sensitivities when the cone aperture is assumed to be the inner segment, and the middle curve when it is assumed to be the outer segment. The experimental conditions and ideal observer characteristics are given in the text and in Table 1.

trast sensitivities are reasonably similar at all eccentricities. In other words, the ideal CSF's do not exhibit the large contrast-sensitivity losses that one observes in humans with increasing eccentricity.

The shapes of ideal CSF's at a given eccentricity are similar for inner- and outer-segment apertures, but the overall sensitivity for inner-segment curves is ~0.5 log unit higher in the periphery. This difference highlights the importance of obtaining more quantitative anatomical data on inner-segment dimensions and shapes so one can calculate the waveguide properties of peripheral cones. In the meantime, one can only estimate ideal contrast sensitivity in the periphery to within 0.5 log unit.

The similarities and dissimilarities between human and ideal performance are highlighted in Fig. 6. Each panel plots human and ideal CSF's, different panels representing different eccentricities. There are two ideal observer functions in each panel: the upper for inner-segment apertures and the lower for outer-segment.

Human contrast sensitivity in the periphery approaches ideal most closely at intermediate spatial frequencies. With increasing eccentricity, the frequency of that closest point occurs at progressively lower values. In the fovea, human and ideal sensitivity become more similar with increasing spatial frequency up to roughly 4 cpd, after which the difference becomes roughly constant.[11]

Figures 7 and 8 display the ratios of human to ideal sensitivity at various spatial frequencies and eccentricities. We call these neural efficiency plots because they represent the differential efficiency of postreceptor circuits as a function of spatial frequency and eccentricity. Figure 7 is based on ideal observer calculations assuming inner-segment apertures, and Figure 8 is based on calculations assuming outer segments. The left-hand panels show these plots for observer ABS at 0, 5, 10, 20, and 40 deg; the right-hand panels show them for SJA at 2, 10, and 40 deg. Peripheral neural efficiencies are similar at low spatial frequencies: The maximum deviation is less than 0.3 log unit. At higher frequencies neural efficiencies are quite dependent on eccentricity: With increasing retinal eccentricity, efficiency falls off at progressively lower spatial frequencies. Foveal efficiencies appear to differ from these trends. At high spatial frequencies foveal efficiencies are relatively flat, and these are the

highest efficiencies obtained for any eccentricity. At lower spatial frequencies foveal efficiencies are similar to or lower than peripheral efficiencies, but this observation may be artifactual for the following reason. The experiment involved measuring contrast sensitivities at each spatial frequency for an equivalent number of cycles (see Table 1). At low spatial frequencies the standard deviations of the Gabor patch were 0.6–1.0 deg for the foveal measurements, so low-frequency patches were larger than the foveola. At higher spatial frequencies standard deviations were smaller, so these stimuli were presumably confined to the foveola. The largest changes in photoreceptor and lattice properties across the retina occur between 0 and 2 deg (see Figs. 1 and 2), and these changes are detrimental to sensitivity. The ideal observers, on the other hand, were constructed separately for each eccentricity, so lattice properties were constant regardless of patch size. Consequently, human sensitivity was degraded by peripheral intrusion but ideal sensitivity was not. This in turn caused a decrease in the estimated neural efficiency (the ratio of human-to-ideal sensitivity) at low frequencies.

Although the explanation outlined above seems the most plausible for the disparity between foveal and peripheral efficiency at low frequencies, it is also possible that eccentricity-dependent changes in spatial antagonism produced the disparity. Specifically, greater spatial antagonism among foveal retinal ganglion cells would cause more pronounced low-frequency attenuation in the foveal data.

The constancy of foveal efficiencies at high frequencies was reported previously.[11,22] In the present experiment neural efficiency (the ratio of human/ideal sensitivity) in the fovea asymptoted at a value of ~0.06, significantly lower than the value of 0.3–0.5 obtained in previous experiments.[22] Such efficiencies, however, depend critically on stimulus parameters and the psychophysical task. Crowell and colleagues[22] obtained the highest efficiencies by using small Gabor patches and a contrast-discrimination task. The values shown in Figs. 7 and 8 are larger because they are based on the detection, rather than the discrimination, of relatively large patches.

Estimates of neural efficiency depend on whether one assumes that the inner or the outer segments are the effective cone aperture, more so in the periphery than in the fovea. The efficiency estimates are roughly 0.5 log unit higher from 2–40 deg eccentric when outer segments are assumed. Nonetheless, efficiencies are remarkably constant across the visual field at the lowest frequencies tested. For example, at 0.25 cpd the neural efficiencies of observer ABS range from 0.014 to 0.025, assuming outer-segment apertures from 5 to 40 deg eccentric. Efficiencies at higher frequencies obviously vary greatly: With greater eccentricity they plummet at progressively lower spatial frequencies.

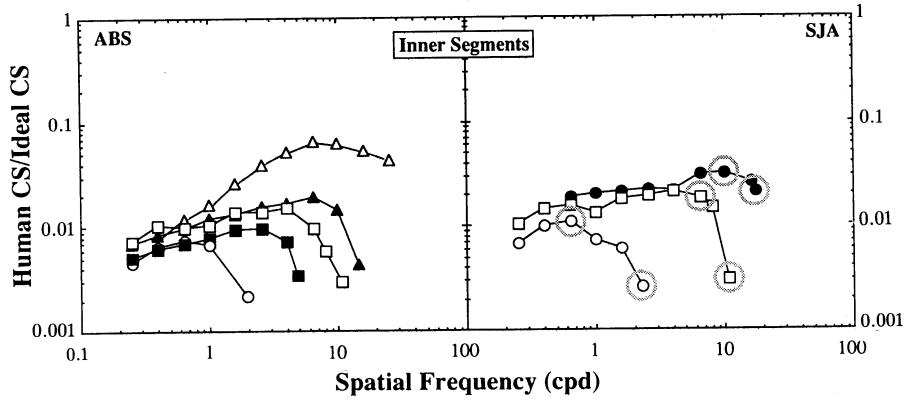

Fig. 7. Neural efficiency functions at different eccentricities, assuming inner-segment apertures. The ratio of human to ideal contrast sensitivity is plotted as a function of spatial frequency. The left- and right-hand panels display these functions for observers ABS and SJA, respectively. The same symbol conventions as in Fig. 4 are used. The circled points in the right-hand panel are the points used to estimate pooling areas (see the Discussion section).

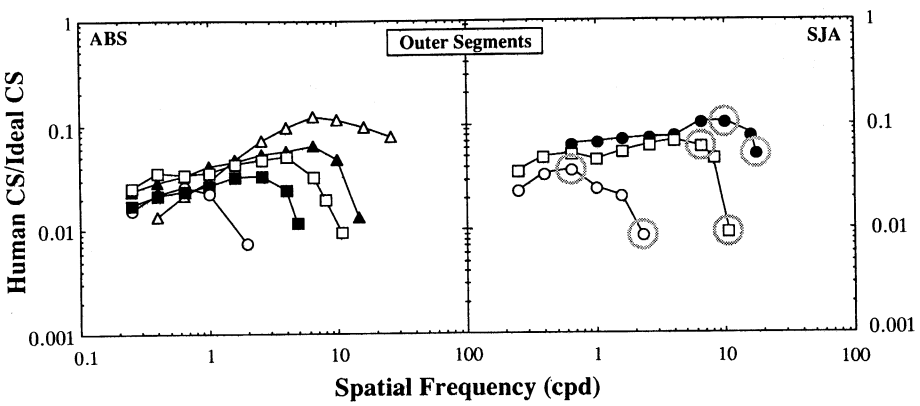

Fig. 8. Neural efficiency functions at different eccentricities, assuming outer-segment apertures. Again the ratio of human to ideal contrast sensitivity is plotted as a function of spatial frequency. The left- and right-hand panels display these functions for observers ABS and SJA, respectively.

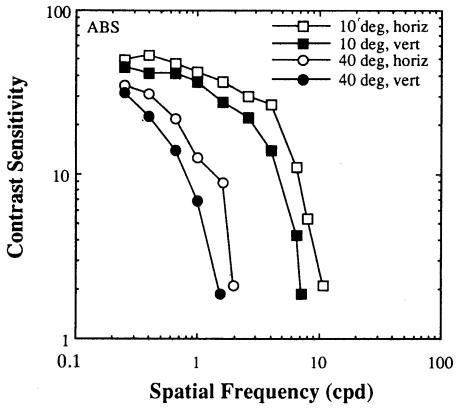

Fig. 9. CSF's for vertical and horizontal gratings presented at eccentricities of 10 and 40 deg. The open symbols represent data for horizontal (radial) gratings, and the filled symbols data for vertical (tangential) gratings. The experimental conditions are described in the text and in Table 1.

EXPERIMENT 3

Experiments 1 and 2 used horizontal gratings only. In Experiment 3 we examined how stimulus orientation affects contrast sensitivity in the periphery.

The oblique effect is well known in foveal vision. In the periphery, the oblique effect gives way to a meridional effect: Grating acuity, for example, is best for gratings oriented radially rather than tangentially with respect to the fovea.[23,24] Meridional effects are also observed among various hyperacuity tasks in the periphery: Bisection acuity is better when the dots are oriented tangentially, so the offset is tangential with respect to the fovea, than when the dots are oriented radially and the offset is radial.[25] Although image formation in the periphery is subject to astigmatism of oblique incidence,[26] these meridional effects are not caused by orientation-specific optical errors.[24,25] They also cannot be attributed to the geometry of the receptor lattice because that geometry is essentially isotropic.[2] For these reasons, meridional variations in peripheral resolution must be caused by anisotropies in postreceptoral circuits. We measured stimulus orientation effects in one observer at eccentricities of 10 and 40 deg in order to examine the magnitude of such anisotropies.

Methods

Vertical grating patches were presented along the horizontal meridian in the nasal visual field. Except for the 90-deg change in stimulus orientation, the stimuli and the procedure were identical to those of Experiment 2.

Results

Figure 9 displays the peripheral CSF's of one observer for vertical and horizontal gratings. As expected,[23,24] a modest, but consistent, meridional effect was observed. At higher spatial frequencies in particular, contrast sensitivity was lower for vertical (tangential) than for horizontal (radial) gratings. This effect was somewhat larger at 40 deg eccentric.

We calculated neural efficiencies, and, as one would predict from Fig. 9, efficiencies above some spatial frequency are lower for tangential than for radial gratings. The lowest spatial frequencies at which radial and tangential efficiencies differ by more than 0.2 log unit are 4 cpd at 10 deg eccentric and 1 cpd at 40 deg.

EXPERIMENT 4

We used ophthalmic lenses and carefully aligned 1.5-mm artificial pupils in Experiments 2 and 3 in an attempt to eliminate focus errors and spherical and chromatic aberrations and thereby render the optics diffraction limited. Recent reports, however, have shown that lateral chromatic aberration can be quite pronounced in the periphery.[27-29] Consequently we were concerned about overestimating the quality of peripheral optics for our viewing conditions. To look for contamination by lateral chromatic aberration, we made some contrast-sensitivity measurements under spectrally broadband and narrow-band conditions. Image degradation caused by lateral chromatic aberration has to be more pronounced for broadband lights, so we reasoned that any ill effects of chromatic aberration would be manifest in the comparison of contrast sensitivity in the two spectral conditions.

Methods

Horizontal and vertical Gabor patches were presented at 10 and 40 deg in the nasal visual field. In the narrow-band condition the observer viewed the stimuli through a Wratten 57 filter (dominant wavelength 540 nm, half-

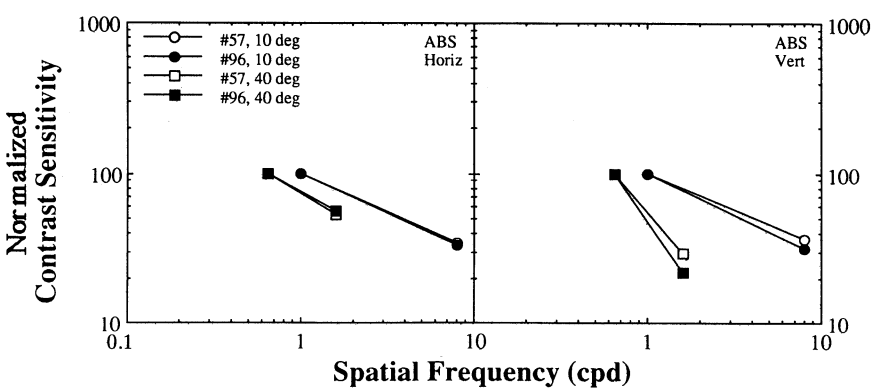

Fig. 10. Contrast sensitivity with spectrally narrow-band and broadband lights. The left- and right-hand panels display data for horizontal (radial) and vertical (tangential) gratings, respectively. The filled symbols represent data with the broadband light (P4 phosphor viewed through a Wratten 96 neutral-density filter). The open symbols represent data with the narrow-band light (P4 viewed through a Wratten 57 filter). The circles and squares represent data at 10 and 40 deg eccentric, respectively. The experimental conditions are described in the text.

width at half-height 37 nm). In the broadband condition the observer viewed the stimuli through a neutral filter. Retinal illuminance was 851 Td in both conditions. Sensitivity to a low and a high spatial frequency was tested at both eccentricities: 0.65 and 1.6 cpd at 10 deg and 1.0 and 8.0 cpd at 40 deg. If lateral chromatic aberration affected the measurements in Experiments 2 and 3, one would expect sensitivity at high frequencies with broadband lights to be lower than with narrow-band lights.

Results

Figure 10 displays the results for horizontal (radial) and vertical (tangential) gratings in the left- and right-hand panels, respectively. Contrast sensitivity for horizontal gratings is essentially identical for the narrow-band and broadband stimuli. This proves that lateral chromatic aberration did not affect thresholds for horizontal gratings in Experiments 1–3. Contrast sensitivity for vertical gratings is slightly higher for narrow-band stimuli but only at higher spatial frequencies. This shows that some of the orientation effect observed in Experiment 3 (see Fig. 9) is due to chromatic aberration. We hasten to point out, however, that the orientation effect in Experiment 3 is much larger than the spectral effect in Fig. 10, so most of the orientation effect must be due to anisotropies among neural mechanisms.

DISCUSSION

The main findings in the present paper are highlighted by the neural efficiency plots of Figs. 7 and 8. Neural efficiency was computed by first constructing ideal observers with the optical and photoreceptor properties of various retinal eccentricities and then comparing ideal and human performance. These comparisons revealed that neural efficiency across the visual field is constant at low spatial frequencies but varies dramatically at intermediate and high frequencies.

We now discuss how receptor pooling might affect neural efficiency and how anisotropies in pooling might affect efficiency for different stimulus orientations. The discussion of pooling is then related to recent anatomical measurements of cone-to-ganglion cell convergence. Next we consider how eccentricity-dependent changes in front-end properties might affect performance in different sorts of spatial tasks, particularly spatial summation and grating and vernier acuity. Finally, we ask whether our findings support the notion that visual pathways subserving central vision are specialized for fine-detail vision.

Receptor Pooling

Banks *et al.*[11] found that neural efficiency was constant from 5 to 40 cpd in foveal vision. They argued that constant neural efficiency implies that information from individual cones is preserved in foveal vision. This implication is consistent with the observation that there is no convergence or pooling of foveal cones onto higher-order retinal neurons, such as retinal ganglion cells.[4]

It is evident from Figs. 7 and 8 that neural efficiency functions in the periphery are not at all flat. Convergence or pooling of cones onto higher-order neurons, which is the rule in the periphery,[4] is a likely contributor to the high-frequency roll-offs in the peripheral efficiency plots. Pooling increases the diameter of the effective sampling unit. By virtue of the inverse relationship between sampling unit size and bandwidth,[30] the larger diameter reduces sensitivity to higher spatial frequencies. The sampling units of our ideal observers were individual cones, so the ideal contrast sensitivities used to calculate the efficiency plots of Figs. 7 and 8 do not reflect the consequences of receptor pooling. This is one reason that they exhibit progressively better high-frequency sensitivity in the periphery than do human observers.

Table 2. Estimated Sampling Unit Diameter (min)

		Eccentricity (deg)				
Observer	Fovea	2	5	10	20	40
ABS	0.48	–	4.26	5.76	11.82	30.36
SJA	0.48	1.8	–	6.21	–	24.78

We hypothesized that receptor pooling is the sole determinant of the high-frequency roll-off in the neural efficiency plots. To pursue this idea, we calculated how much pooling has to be added to the various ideal observers to flatten the efficiency plots at each eccentricity. Specifically, we found how much pooling was required to equate efficiency at two spatial frequencies: the highest one at which a threshold could be measured and the one at which efficiency was highest (see Figs. 7 and 8). We did this by constructing ideal observers with cylindrical sampling units of different diameters. We then found the diameter required to reduce ideal high-frequency sensitivity enough to flatten the various neural efficiency plots. Those diameters are given in Table 2. Note that the diameters of the sampling units increase by more than a factor of 50 from the fovea to 40 deg eccentric. Figure 11 displays neural efficiencies calculated with ideal observers with these larger sampling units. Notice that the ratios of human to ideal contrast sensitivity are nearly constant across spatial frequencies and eccentricities. Constant efficiency across spatial frequencies was manufactured because we manipulated the diameter of the sampling units to achieve this. But constant efficiency across eccentricities was not manufactured, and this observation suggests that the ability of postretinal mechanisms to transmit contrast information may be constant across the visual field once the consequences of optics, photoreceptor properties, and pooling are taken into account. We return to this point below.

Before considering whether the pooling estimates correspond to any particular anatomical observation (such as cone-to-ganglion cell convergence[4]), we consider whether the performance of ideal observers with pooling is consistent with other data. Ricco's critical diameter is an index of the spatial extent of complete summation and should be sensitive to pooling effects. We examined whether critical diameters for ideal observers with the pooling given in Table 2 are similar to the diameters actually observed at different eccentricities.

Wilson[31] measured increment thresholds as a function of test spot diameter at eccentricities of 5–50 deg. We used these measurements to calculate critical diameters at 5, 10, 20 and 40 deg. Wilson did not measure critical diameter in the fovea, so we used data from Davila and Geisler.[32]

Figure 12 shows how we estimated critical diameters for human and ideal observers. The left-hand panel is a replot of Wilson's results at 40 deg; the two lines fitted to the data have slopes of −2 (indicating the region of com-

plete summation or Ricco's law) and −1 (indicating the region of partial summation). Critical diameter was defined as the intersection of these lines. Because the data did not conform perfectly to lines with slopes of −2 and −1, we tried a range of fits to see how accurately the intersection could be identified. The fits were generally significantly poorer if the intersection was changed by ±0.1 log unit. The right-hand panel shows the same analysis for ideal observer data at 40 deg with receptor pooling. Again, critical diameter is the intersection of the best-fitting lines with slopes of −2 and −1.

Figure 13 displays human and ideal critical diameters as a function of eccentricity. The circles represent psychophysical results from Wilson's and Davila and Geisler's experiments. The thick solid and dashed curves represent ideal observer results with pooling. The similarity between human and ideal critical diameters is remarkable. In both cases, critical diameters range from ~3 min at the fovea to ~23 min at 40 deg. The similarity of human and ideal critical diameters across the visual field illustrates the linkage between high-frequency contrast sensitivity and spatial summation. It also shows that the performance of ideal observers with the optics and receptor properties of different retinal regions and with different amounts of receptor pooling depending on eccentricity is closely similar to human performance at different eccentricities, except for a shift in overall sensitivity.

We have shown that some amount of pooling renders neural efficiency plots constant across the visual field and that the same amount of pooling renders ideal and human critical diameters the same at various eccentricities. There is no obvious way to determine from psychophysical data alone whether the pooling required to achieve these ends corresponds to the convergence of cones onto a particular anatomical site, but it is important to ask whether these indirect means of estimating pooling are consistent with specific anatomical–physiological findings.

Recently Wässle *et al.*[33] and Curcio and Allen[4] estimated cone-to-ganglion cell ratios from macaque and human retinal tissue, respectively, at various eccentricities. Figure 14 plots their anatomically based estimates of cone-to-ganglion cell ratios and our psychophysically based estimates of the ratio of cones to higher-order neurons at some unknown site. Notice that the anatomical ratios are systematically lower than the psychophysical ratios. Consider the possibility that retinal ganglion cells are the site corresponding to the effective sampling units. Then the most obvious prediction—that each cone connects to one and only one ganglion cell sampling unit (but that a ganglion cell might receive input from more than one cone)—is disconfirmed. It is likely, however, that there is substantial spatial overlap among ganglion cell (center mechanisms) receptive fields. For example, midget ganglion cells come in two varieties in roughly equal proportions: ON and OFF cells.[35] To create the center mechanisms of ON and OFF subsystems, one should have two ganglion cells per foveal cone. Moreover, there are other morphological and physiological classes of

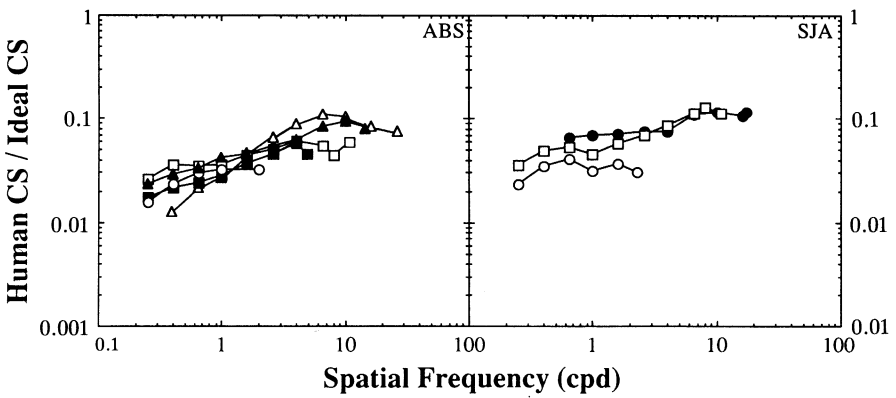

Fig. 11. Neural efficiency functions once pooling is taken into account in the ideal observers. The left- and right-hand panels represent functions from observers ABS and SJA, respectively. The ratio of human to ideal contrast sensitivity is plotted as a function of spatial frequency. The same symbol conventions as in Fig. 4 are used. The procedure for estimating pooling areas is described in the text.

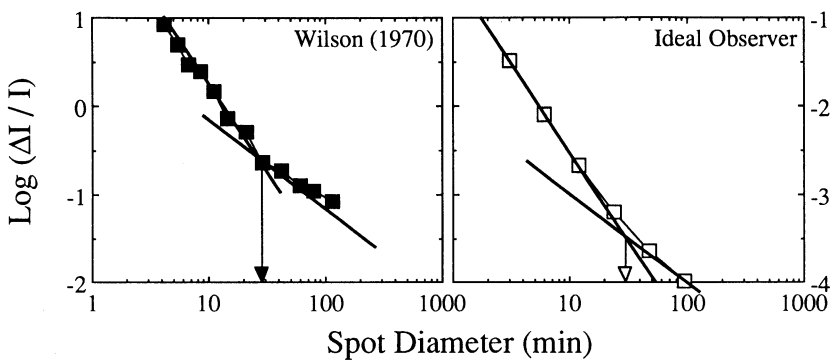

Fig. 12. Procedure for estimating Ricco's critical diameter for human and ideal observers. Increment threshold is plotted as a function of target diameter. The left-hand panel displays data from Wilson,[31] and the right-hand panel the corresponding ideal observer thresholds. The background illuminance in Wilson's experiment was 1200 Td, and the pupil diameter was 3 mm. The two lines fitted to the data have slopes of −2 (complete summation) and −1 (partial summation). The arrows indicate the intersections of the two lines.

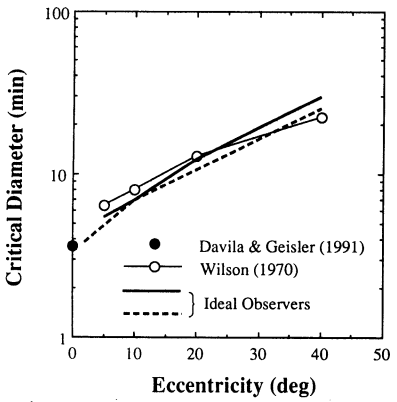

Fig. 13. Ricco's critical diameter at different eccentricities. The circles represent critical diameter estimates from increment threshold experiments of Davila and Geisler[32] and Wilson.[31] The solid and dashed curves represent critical diameter estimates from ideal increment threshold calculations (again see Fig. 12). Two functions are displayed—one for observer ABS and one for observer SJA—because different pooling estimates were obtained for the two observers.

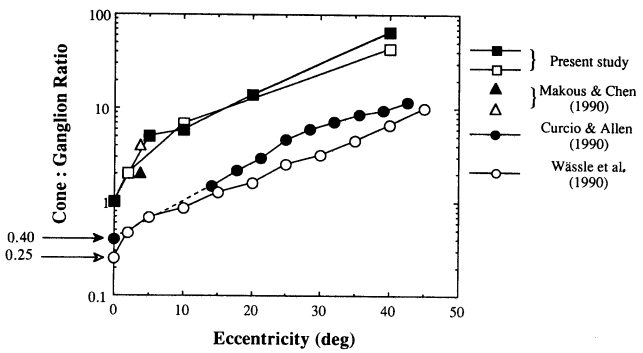

Fig. 14. Anatomical and psychophysical pooling estimates. The number of cones per ganglion cell is plotted at a variety of eccentricities. The squares and triangles represent psychophysical estimates from the present study and from Makous and Chen,[34] respectively. The ordinate values—again the number of cones per ganglion cell—were obtained by first estimating the diameter and the area of effective sampling units and then finding the number of cones that (according to Curcio *et al.*[2]) would be required to fill such an area.

ganglion cell in the primate retina,[35] so it is likely that there are more than two ganglion cells per foveal cone. Consistent with this idea, Curcio and Allen[4] report a ratio of two to four ganglion cells per cone in the human foveola, and Wässle *et al.*[33] report a ratio of four to one in the macaque foveola. From previous studies[11] we assume that the effective cone-to-sampling-unit convergence ratio is 1:1. So we examined the idea that reducing the anatomical ratios by a factor of 4 would make the anatomical and psychophysical estimates similar. We assume in using a common shift factor for all eccentricities that the overlap of ganglion cell receptive fields is reasonably constant across the visual field, as it is in cats.[36] As Fig. 15 shows, the correspondence between the psychophysical estimates of sampling unit size and the shifted anatomical estimates of convergence ratios is reasonably good. The largest deviation between psychophysics and Curcio and Allen's human anatomy is less than 0.2 log unit. The reasonable correspondence suggests that ganglion cell center mechanisms are the sampling units revealed in our psychophysical measurements.

Effects of Grating Orientation

In Experiment 3 we examined how stimulus orientation affects peripheral contrast sensitivity. In previous studies[23,24] and in our experiments the high-frequency limbs of peripheral CSF's fell more rapidly when the target gratings were oriented tangentially. This meridional effect cannot be understood from an analysis of information available at the cone outputs because the optics were nearly isotropic in our experimental situation and because the cone lattices are essentially isotropic at each of the eccentricities that we investigated.[2] Therefore, the meridional effect in grating acuity and hyperacuity must be caused primarily by postreceptoral anisotropies.

There is substantial evidence that cone pooling onto retinal ganglion cells is anisotropic in the mammalian visual system.[37,38] Specifically, pooling is greater radially than tangentially with respect to the fovea. In the analysis that went into the construction of Table 2 and Figs. 13–15 we made the unlikely assumption that pooling was isotropic at each retinal eccentricity. We now examine this assumption by asking how much anisotropy in cone pooling has to be added to ideal observers in order to produce flat efficiency plots for radial and tangential gratings simultaneously. Figure 16 summarizes the results for tangential and radial gratings. Notice that, at both eccentricities tested, more pooling is required for tangen-

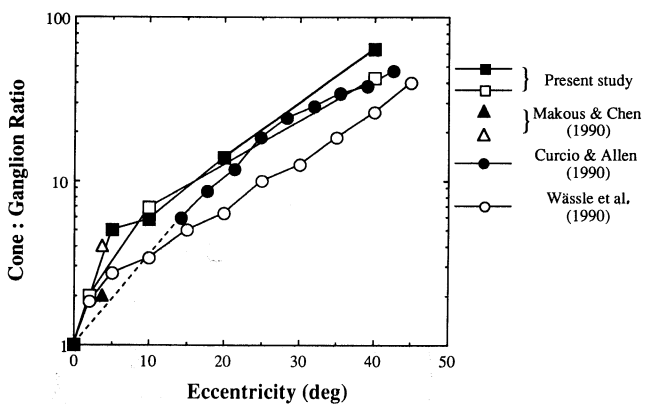

Fig. 15. Psychophysical and shifted anatomical pooling estimates. The same symbols conventions as in Fig. 14 are used. The anatomical estimates have been shifted upward by a factor of 4, a factor that brings the foveal ratio to 1:1.

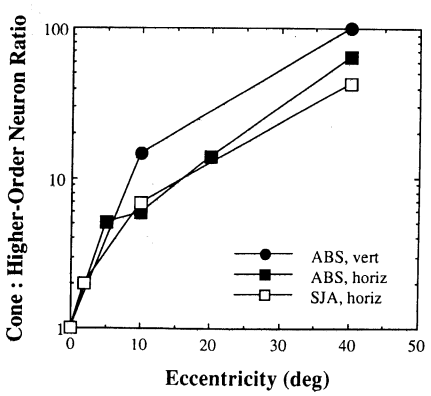

Fig. 16. Psychophysical pooling estimates as a function of orientation. The squares represent estimates from horizontal (radial) gratings, and the circles estimates from vertical (tangential) gratings. The ordinate values were obtained by first estimating the diameter of effective sampling units and then finding the number of cones required to fill such a sampling unit.

tial gratings, a result that agrees qualitatively with the anatomical finding that cone pooling onto retinal ganglion cells is greater in radial directions than in tangential. Unfortunately, we cannot evaluate how well these estimates agree with anatomical estimates of anisotropies in cone pooling because none of the human anatomical data have been examined for such anisotropies.

Aliasing

Unlike the situation for foveal vision, the optical quality of the periphery theoretically exceeds the sampling frequency of the cone lattice.[1] Thus it is not surprising that low-frequency distortion products (aliasing) resulting from undersampling can be observed in the periphery under conventional viewing conditions.[39,40] All the spatial frequencies tested in our experiments were below the theoretical Nyquist limit imposed by the cone sampling lattice and probably below the limit imposed by postreceptor sampling.[41] Not surprisingly, then, we did not observe aliasing in any of our experimental conditions. The evidence for this is that both observers were able to determine the orientation of the grating targets at detection threshold.

Grating and Vernier Acuity

In many visual resolution tasks the observer is asked to report the displacement of a feature relative to one or more other features (e.g., vernier, bisection, separation). In other tasks the observer is simply asked to report the presence of a patterned stimulus as opposed to a uniform field (e.g., grating acuity). Performance in displacement tasks declines more rapidly with eccentricity than does performance in grating acuity tasks.[8,9,42] Westheimer[8] pointed out that the diverse effects of eccentricity on vernier and grating acuity rule out the possibility that central and peripheral spatial vision are the same except for a single spatial scaling factor. Levi and colleagues[9] expanded this argument by asserting that different structures must limit the two forms of acuity. The variation in grating acuity with position in the visual field, they argued, is due mostly to optical blur[1] and to retinal factors such as decreasing cone density.[2,3] In contrast, the variation in the hyperacuities is supposedly due to cortical factors, specifically, the eccentricity-dependent mapping between visual space and the striate cortex known as cortical magnification.[5,43,44] In support of their thesis, Levi and colleagues showed that normalized grating acuity varied with position in the visual field as cone density does, whereas normalized vernier acuity thresholds varied as cortical magnification does.

As we described above, optical, receptor, and other retinal properties vary in many ways across the retina. The OTF of the eye slowly becomes poorer with increasing eccentricity,[1] cone density declines more rapidly and nearly linearly,[2,3] outer segment length decreases precipitously in the central 2 deg and slowly thereafter,[15,16] and the convergence of cones onto retinal ganglion cells increases slowly and steadily across the whole retina.[4] These factors are bound to influence performance in spatial visual tasks, probably in different ways in different tasks. Thus the hypothesis of Levi and his colleagues—that optical and retinal factors alone cause the eccentricity-dependent variations in grating acuity (and other related tasks) while cortical magnification alone causes similar variations in vernier acuity (and related tasks)—may be too simple.

We used ideal observer analyses to examine how front-end properties—optics and photoreceptor spacing, efficiency, and pooling onto higher-order retinal neurons—might contribute to peripheral grating and vernier acuity. The motivation came from work of Geisler and Davila,[45] who showed that ideal two-dot resolution acuity is less affected than two-dot separation acuity by the number of available photons: Resolution followed quarter-root law (a 4-log-unit decline in luminance was required for reduction in acuity by a log unit), whereas separation followed square-root law.

To examine how front-end properties affect grating and vernier acuity at different eccentricities, we presented stimuli like those in an experiment by Westheimer[8] to our ideal observers. Westheimer measured both acuities at eccentricities of 0, 2.5, 5, and 10 deg. Grating acuity was measured with square-wave gratings covering a square area of side length equal to 6 cycles. Vernier acuity was measured with two small dots whose separation was optimal for the eccentricity being tested. The left-hand panel of Fig. 17 displays his results. Vernier acuity falls off approximately twice as much as grating acuity over the span of eccentricities tested. The luminance of Westheimer's targets was increased for the peripheral conditions. We held luminance fixed in our ideal observer calculations, which are shown in the right-hand panel.[46] Outer-segment apertures were assumed in constructing the right-hand panel, but much the same picture emerges when inner-segment apertures are assumed. The open symbols represent thresholds for the ideal observers without pooling, and the filled symbols thresholds with pooling. The thresholds have been shifted vertically to aid comparison with Westheimer's data. Ideal vernier thresholds with and without pooling fall off more rapidly than grating thresholds with eccentricity.[47] The eccentricity dependence of ideal observer performance with pooling is similar to that of Westheimer's data: Both ideal and human vernier thresholds fall off more rapidly with eccentricity than do grating thresholds.

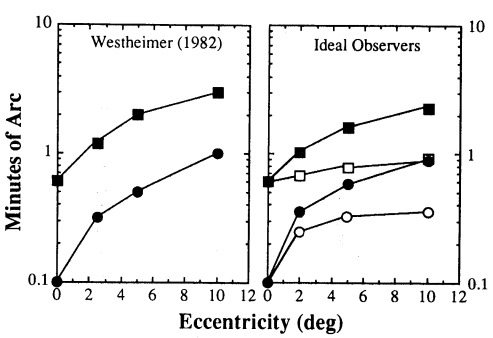

Fig. 17. Human and ideal grating and vernier acuity as a function of eccentricity. The left-hand panel displays the results of Westheimer.[8] The right-hand panel displays ideal grating and vernier acuity for the same stimulus conditions. In both panels the just-discriminable vernier offset is represented by the circles and the just-detectable grating bar width is represented by squares. The points in the right-hand panel have been shifted vertically to ease comparison with Westheimer's data. The open symbols in the right-hand panel represent thresholds for ideal observers without pooling, and the filled symbols ideal thresholds with pooling.

These analyses show that a greater degradation of vernier acuity with eccentric viewing is expected from known variations in front-end mechanisms. Thus models that postulate different neural mechanisms as the limiting factors in different acuity tasks (e.g., retinal factors for grating and central factors for vernier) are probably too simple. We are not arguing that front-end properties alone are sufficient for an understanding of how the acuities change with eccentricity, because many psychophysical observations are inconsistent with ideal observer performance.[48] Rather, we are arguing that the discrimination information available at the retinal ganglion cells varies with eccentricity and, more importantly, that the information relevant to vernier acuity declines more rapidly with eccentricity than does the information for grating acuity. The differing impact of front-end limitations for different spatial visual tasks should be incorporated into any model of how anatomical/physiological structures constrain performance.

Postretinal Efficiency of Foveal and Peripheral Vision

The fovea is clearly specialized for fine-detail vision. Foveal cones are tightly packed, so the sampling frequency is much higher than elsewhere. Moreover, there are more bipolar and retinal ganglion cells in the fovea than there are cones, so information from single cones can be preserved in the outputs of the retina. But, aside from these retinal specializations, do central visual circuits treat information from foveal and peripheral cones differently? Until recently, the conventional wisdom was that central circuits overrepresent the fovea relative to the rest of the visual field. This view was quantified by the difference between retinal and cortical magnification factors.[9,43] More recent anatomical measurements, however, suggest little if any difference between retinal and cortical magnification.[4,33] Our results are compatible with these recent measurements. Consider, for example, the efficiency functions in Fig. 11. These functions are the ratio of human contrast sensitivity divided by the contrast sensitivity of ideal observers with the optics, photoreceptors, and pooling characteristic of different retinal eccentricities. Except for a deviation between foveal and peripheral efficiencies at low frequencies, which is due to experimental artifact (see the discussion of Experiment 2), the ratio of human to ideal sensitivity is essentially the same for eccentricities of 0 to 40 deg. The observation of similar neural efficiency functions in Fig. 11 suggests that postretinal mechanisms are equally proficient at signaling contrast information in the fovea and periphery. Thus the greater contrast sensitivity and resolving power of the fovea may result from optical and retinal specializations only.

ACKNOWLEDGMENTS

We thank Christine Curcio for providing preprints of her data on human cone dimensions and cone-to-ganglion-cell convergence, Bill Geisler for assisting us in installing his SDE software, Stan Klein for the loan of his work station, Chang Cheng-Yu and Rick Van Sluyters for the careful measurements of cone outer-segment dimensions, and Walt Makous for providing preliminary data on his measurements of cone apertures and peripheral receptor pooling. This research was supported by National Institutes of Health research grant HD-19927 awarded to M. S. Banks. A. B. Sekuler was the recipient of a University of California Regents Fellowship. S. J. Anderson was the recipient of a Fulbright Fellowship.

*Present address, Department of Psychology, Sydney Smith Hall, University of Toronto, Toronto M5S 1A1, Ontario, Canada.

†Present address, Department of Visual Sciences, Aston University, Aston Triangle, Birmingham B4 7ET, England.

REFERENCES AND NOTES

1. J. A. M. Jennings and W. N. Charman, "Off-axis image quality in the human eye," Vision Res. **21,** 445–451 (1981).
2. C. A. Curcio, K. R. Sloan, R. E. Kalina, and A. E. Hendrickson, "Human photoreceptor topography," J. Comp. Neurol. **292,** 497–523 (1990).
3. G. Oesterberg, "Topography of the layer of rods and cones in the human retina," Acta Ophthalmol. Suppl. **6,** 1–97 (1935).
4. C. A. Curcio and K. A. Allen, "Topography of ganglion cells in human retina," J. Comp. Neurol. **300,** 5–25 (1990).
5. R. B. H. Tootell, E. Switkes, M. S. Silverman, and S. L. Hamilton, "Functional anatomy of macaque striate cortex. II. Retinotopic organization," J. Neurosci. **8,** 1531–1568 (1988).
6. V. Virsu and J. Rovamo, "Visual resolution, contrast sensitivity, and the cortical magnification factor," Exp. Brain Res. **37,** 475–494 (1979).
7. D. H. Hubel and T. N. Wiesel, "Uniformity of monkey striate cortex: a parallel relationship between field size, scatter, and magnification factor," J. Comp. Neurol. **158,** 295–308 (1974).
8. G. Westheimer, "The spatial grain of the perifoveal visual field," Vision Res. **22,** 157–162 (1982).
9. D. M. Levi, S. A. Klein, and A. P. Aitsebaomo, "Vernier acuity, crowding, and cortical magnification," Vision Res. **25,** 963–977 (1985).
10. W. S. Geisler, "Sequential ideal-observer analysis of visual discriminations," Psychol. Rev. **96,** 267–314 (1989).
11. M. S. Banks, W. S. Geisler, and P. J. Bennett, "The physical limits of grating visibility," Vision Res. **27,** 1915–1924 (1987).
12. D. G. Green, M. K. Powers, and M. S. Banks, "Depth of focus, eye size, and visual acuity," Vision Res. **20,** 827–835 (1980).
13. W. S. Geisler, "Physical limits of acuity and hyperacuity," J. Opt. Soc. Am. A **1,** 775–782 (1984).
14. H. H. Hopkins, "21st Thomas Young oration. The application of frequency response techniques in optics," Proc. Phys. Soc. London **79,** 889–919 (1962).
15. S. L. Polyak, *The Vertebrate Visual System* (U. Chicago Press, Chicago, Ill., 1957).
16. C. Cheng-Yu and R. C. Van Sluyters, School of Optometry, University of California, Berkeley, Berkeley, California 94720 (personal communication, 1990).
17. D. I. A. MacLeod, D. R. Williams, and W. Makous, "A visual nonlinearity fed by single cones," J. Opt. Soc. Am. A (to be published).
18. G. Wyszecki and W. S. Stiles, *Color Science: Concepts and Methods, Quantitative Data and Formulae* (Wiley, New York, 1982).
19. J. G. Robson and N. Graham, "Probability summation and regional variation in contrast sensitivity across the visual field," Vision Res. **21,** 409–418 (1981).
20. E. R. Howell and R. F. Hess, "The functional area for summation to threshold for sinusoidal gratings," Vision Res. **18,** 369–374 (1978).
21. W. H. Miller and G. D. Bernard, "Averaging over the foveal receptor aperture curtails aliasing," Vision Res. **23,** 1365–1370 (1983).
22. J. Crowell, M. S. Banks, S. J. Anderson, and W. S. Geisler, "Physical limits of grating visibility: fovea and periphery," Invest. Ophthalmol. Vis. Sci. Suppl. **29,** 139 (1988).

23. J. Rovamo, V. Virsu, P. Laurinen, and L. Hyvarinen, "Resolution of gratings oriented along and across meridans in peripheral vision," Invest. Ophthalmol. Vis. Sci. **23,** 666–670 (1982).
24. L. A. Temme, L. Malcus, and W. K. Noell, "Peripheral visual field is radially organized," Am. J. Optom. Physiol. Opt. **62,** 545–554 (1985).
25. Y. L. Yap, D. M. Levi, and S. A. Klein, "Peripheral hyperacuity: isoeccentric bisection is better than radial bisection," J. Opt. Soc. Am. A **4,** 1562–1567 (1987).
26. C. E. Ferree, G. Rand, and C. Hardy, "Refraction for the peripheral field," Arch. Ophthalmol. **15,** 717–731 (1931).
27. Y. U. Ogboso and H. E. Bedell, "Magnitude of lateral chromatic aberration across the retina of the human eye," J. Opt. Soc. Am. A **4,** 1666–1672 (1987).
28. L. N. Thibos, "Calculation of the influence of lateral chromatic aberration on image quality across the visual field," J. Opt. Soc. Am. A **4,** 1673–1680 (1987).
29. P. Simonet and M. C. W. Campbell, "The optical transverse chromatic aberration on the fovea of the human eye," Vision Res. **30,** 187–206 (1990).
30. A. W. Snyder and W. H. Miller, "Photoreceptor diameter and spacing for highest resolving power," J. Opt. Soc. Am. **67,** 696–697 (1977).
31. M. E. Wilson, "Invariant features of spatial summation with changing locus in the visual field," J. Physiol. **207,** 611–622 (1970).
32. K. D. Davila and W. S. Geisler, "The relative contributions of preneural and neural factors to areal summation in the fovea," Vision Res. **31,** 1369–1380 (1991).
33. H. Wässle, U. Grünert, J. Röhrenbeck, and B. B. Boycott, "Retinal ganglion cell density and cortical magnification factor in the primate," Vision Res. **30,** 1897–1912 (1990).
34. W. Makous and B. Chen, Center for Visual Science, University of Rochester, Rochester, New York 14627 (personal communication, 1990).
35. R. W. Rodieck, "The primate retina," Comp. Primate Biol. **4,** 203–278 (1988).
36. L. Peichl and H. Wässle, "Size, scatter and coverage of ganglion cell receptive field centres in the cat retina," J. Physiol. (London) **291,** 117–141 (1979).
37. A. G. Leventhal and J. D. Schall, "Structural basis of orientation selectivity of cat retinal ganglion cells," J. Comp. Neurol. **220,** 465–475 (1983).
38. J. D. Schall, V. H. Perry, and A. G. Leventhal, "Retinal ganglion cell dendritic fields in old-world monkeys are oriented radially," Brain Res. **368,** 18–23 (1986).
39. R. A. Smith and P. F. Cass, "Aliasing in the parafovea with incoherent light," J. Opt. Soc. Am. A **4,** 1530–1534 (1987).
40. S. J. Anderson and R. F. Hess, "Post-receptoral undersampling in normal human peripheral vision," Vision Res. **30,** 1507–1516 (1990).
41. L. N. Thibos, F. E. Cheney, and D. J. Walsh, "Retinal limits to the detection and resolution of gratings," J. Opt. Soc. Am. A **4,** 1524–1529 (1987).
42. F. W. Weymouth, "Visual sensory units and the minimal angle of resolution," Am. J. Ophthalmol. **46,** 102–113 (1958).
43. B. M. Dow, A. Z. Snyder, R. G. Vautin, and R. Bauer, "Magnification factor and receptive field size in foveal striate cortex of the monkey," Exp. Brain Res. **44,** 213–228 (1981).
44. D. C. Van Essen, W. T. Newsome, and J. H. R. Maunsell, "The visual field representation in the striate cortex of the macaque monkey: asymmetries, anisotropies, and individual variability," Vision Res. **24,** 429–448 (1984).
45. W. S. Geisler and K. D. Davila, "Ideal discriminators in spatial vision: two-point stimuli," J. Opt. Soc. Am. A **2,** 1483–1497 (1985).
46. In most hyperacuity experiments, small bright targets are presented on dim backgrounds. The retinal region being tested is consequently adapted to a much lower luminance than the target, so, on target presentation, the stimulated neurons are probably pushed well into the saturated portion of compressive nonlinearities. Thus one would not expect threshold displacement to change much if the luminance of such targets were varied. Ideal displacement thresholds, on the other hand, follow square-root law, threshold being inversely proportion to the square root of target luminance. So we chose to fix target luminance for the ideal observer calculations displayed in Fig. 17.
47. The differing effects of eccentricity on ideal vernier and grating acuity follow from the observation that ideal vernier acuity is affected more by the number of absorbed quanta than is grating acuity.[45] The quantum catch of the peripheral cone lattice is less than that of the fovea (see Fig. 2), so ideal vernier acuity suffers more.
48. For one thing, vernier acuity seems to be somewhat resilient to reductions in target luminance and to the length of the target elements, etc. [see Ref. 45; G. Westheimer and S. P. McKee, "Spatial configurations for visual hyperacuity," Vision Res. **17,** 941–947 (1977)].